

Dirac topological insulator in the d_{z^2} manifold of a honeycomb oxide

J. L. Lado¹ and V. Pardo^{2,3}

¹*International Iberian Nanotechnology Laboratory, Braga, Portugal*^{*}

²*Departamento de Física Aplicada, Universidade de Santiago de Compostela,*

E-15782 Campus Sur s/n, Santiago de Compostela, Spain

³*Instituto de Investigaciones Tecnológicas, Universidad de Santiago de Compostela,*

E-15782 Campus Sur s/n, Santiago de Compostela, Spain[†]

(Dated: August 30, 2021)

We show by means of ab initio calculations and tight-binding modeling that an oxide system based on a honeycomb lattice can sustain topologically non-trivial states if a single orbital dominates the spectrum close to the Fermi level. In such situation, the low energy spectra is described by two Dirac equations that become non-trivially gapped when spin-orbit coupling (SOC) is switched on. We provide one specific example for this but the recipe is general. We discuss a realization of this starting from a conventional spin-a-half honeycomb antiferromagnet whose states close to the Fermi energy are d_{z^2} orbitals. Switching off magnetism by atomic substitution and ensuring that the electronic structure becomes two-dimensional is sufficient for topologicality to arise in such a system. We show that the gap in such model scales linearly with SOC, opposed to other oxide-based topological insulators, where smaller gaps tend to appear by construction of the lattice. We also provide a study of the quantum Hall effect in such system, showing the close connections with the physics of graphene but in a d-electron system.

I. INTRODUCTION

Topological insulators^{1,2} (TI) are a new class of materials that present a gap in the bulk but on their edges they have gapless states that conduct without dissipation. They have produced a renewed understanding of the topological properties of the single-particle Hamiltonian that describes the electronic structure of an insulator. The topological properties of the edge states arise due to a finite Chern number as in the quantum Hall effect,^{3,4} they can be protected by different symmetries of the Hamiltonian, such as crystalline⁵ or time reversal symmetry,⁶ or they can be arise due to interaction effects in topological Mott insulators⁷ and topological Kondo insulators.⁸ Among the different possible classes, TI with time reversal (TR) symmetry¹ show spin-momentum locking in their edge states. All sorts of peculiar physics has been predicted to arise from them, such as topological superconductors showing² Majorana bound states⁹ with anyonic statistics.¹⁰ In terms of applications, those dissipation-less edge state could help in transmitting information without losses,¹¹ find applications in spintronic devices¹² or become a key ingredient for topological quantum computing.^{9,13}

Topological insulators can appear in two or three dimensional systems. In two-dimensions, the first proposal for a topological insulator was the prediction of a quantum spin Hall effect,¹⁴ a peculiar type of quantum Hall effect that is not caused by an external magnetic field but by the internal spin-orbit interaction of the material. This was first proposed to appear in graphene¹⁵ but not materialized experimentally. The same ideas were shown to operate in HgTe/CdTe quantum wells,¹⁶ where a larger SOC strength takes place and allowed for its experimental observation.¹⁷

Oxides provide also an interesting platform for non-

trivial topological properties to appear. Early since the discovery of topological insulators, several oxides with different structures have been identified as possible topological insulators: honeycomb-based iridates,¹⁸ pyrochlores,¹⁹ corundum structure^{20,21} and rutiles.^{22,23} The honeycomb lattice has been the simplest to investigate. Based on these concepts, Xiao et al.²⁴ proposed to build an oxide-based honeycomb lattice, though largely buckled, using perovskite bilayers grown along the perovskite (111) direction, and other authors have followed suit, showing that this kind of phases appear ubiquitously, even for the low SOC limit.²⁵ It was shown²⁶ that the size of the topological gap depends on the strength of the trigonal splitting, and only inversely with SOC strength, hence these phases show up also for 3d electron systems, but there they compete with Jahn-Teller distortions, charge and magnetic ordering.^{21,24,26}

Here we propose a different oxide-based route to realize topologically non-trivial properties. The system under study shows a low-energy electronic structure identical to the one of graphene, but with d_{z^2} orbitals dominating the spectrum around the Fermi level instead of the p_z states of graphene. Our proposal is based of atomic substitution on the recently synthesized compound $\text{InCu}_{2/3}\text{V}_{1/3}\text{O}_3$,²⁷⁻²⁹ which shows a honeycomb lattice of $\text{S}=1/2$ Cu^{2+} cations. We propose to substitute Cu by isoelectronic Ag^{30} and isolate the active Ag-rich planes by a Zn-rich layer to produce a truly two-dimensional electronic structure. In $\text{InZn}_{1/3}\text{Ag}_{1/3}\text{V}_{1/3}\text{O}_3$, due to the interplay of local C_3 symmetry, crystal field and charge transfer, close to the Fermi energy the band structure is composed by Ag d_{z^2} orbitals forming an effective honeycomb lattice. In the absence of SOC, the low-energy spectrum is described by two gapless Dirac equations close to the K and K' points. When relativistic effects are included, the system opens

up a gap and shows a topological invariant $\nu = -1$, realizing the quantum spin Hall effect as a d_{z^2} version of the Kane-Mele model.¹⁵ We show that the quantum spin Hall effect is resilient to certain time reversal symmetry breaking, such as off-plane magnetism and gauge magnetic fields. We also show that the gauge magnetic field yields a ferromagnetic quantum spin Hall state, showing the Landau level structure typical of Dirac fermions. Finally, we summarize our conclusions.

II. ELECTRONIC STRUCTURE ANALYSIS

A. Antiferromagnetic Cu based compound

We start describing the electronic structure of the recently synthesized compound $\text{InCu}_{2/3}\text{V}_{1/3}\text{O}_3$,²⁷ which is formed by a honeycomb lattice of $S=1/2$ Cu^{2+} cations developing an antiferromagnetic order. Even though its structure (see Fig. 1a) looks very complicated, composed by alternating layers of In and Cu,V within an oxygen environment, its electronic structure turns out to be very simple. With a simple ionic model one can do the following electron count: In^{3+} , V^{5+} : d^0 (both full/empty shell ions) and Cu^{2+} : d^9 ($S=1/2$). The local environment of Cu is CuO_5 , with the z-axis being a C_3 symmetry axis and the three in-plane oxygens forming 120° (see Fig. 1b,c). In this situation the d_{z^2} orbitals lie higher in energy, half filled, whereas the other d-orbitals are completely filled. Therefore, close to the Fermi level, only the higher-lying d_{z^2} orbitals are present, substantially separated and electronically decoupled from all other d orbitals. This gives rise to an effective single orbital weakly coupled pair of honeycomb lattices, one per each Cu plane in the unit cell (Fig. 1d). This decoupling of the d_{z^2} bands can be understood by the local C_3 symmetry, which allows to expand the polar dependence of the local potential as $V_{C_3}(r, \theta, \phi) = \sum_n a_n e^{i3\phi n} v_n(r, \theta)$, with ϕ the polar angle. The previous expansion guarantees that locally there is no mixing between $d_{z^2}(m=0)$ and the other d-orbitals ($m=\pm 1$ i.e. the xz/yz orbitals, ± 2 i.e. the xy/x^2-y^2 ones), given that any matrix element of the form $\langle m=0 | e^{i3\phi n} | m=\pm 1, \pm 2 \rangle$ is identically zero for $n \neq 0$. This can be seen in Fig. 1e, where the band structure of the antiferromagnetic Cu-based system is presented and the bands both just above and below the Fermi level have Cu d_{z^2} symmetry. Thus, to some extent, such a complicated material like $\text{InCu}_{2/3}\text{V}_{1/3}\text{O}_3$ turns out to be effectively a single-band compound. Opposite to high- T_c cuprates, where the $d_{x^2-y^2}$ band occurs around the Fermi level, here it is the d_{z^2} band that is central. The nearest-neighbor antiferromagnetic coupling produces a 2D-AF, which is the ground state even without correlations due to the low bandwidth of the Cu d_{z^2} bands. Experimentally, a large $J_{AF} = 120$ K has been estimated, with a magnetic phase transition of some sort occurring at 38 K.²⁷

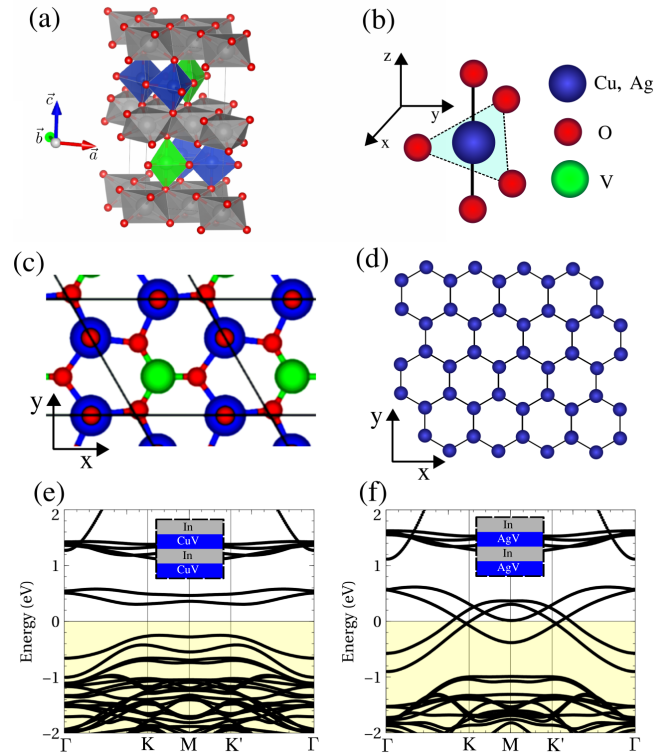


FIG. 1. (Color online.) (a) Unit cell of the crystal, showing alternating planes of Cu(Ag),V and In. Panel (b) shows a sketch of the Cu(Ag) oxygen environment, giving rise to local C_3 symmetry. Panel (c) shows the Ag,V plane, where the Ag atoms form a (slightly distorted) honeycomb lattice as shown in (d). Panel (e) shows the band structure of $\text{InCu}_{2/3}\text{V}_{1/3}\text{O}_3$ calculated at the GGA level, yielding a gapped antiferromagnetic ground state. In comparison, for $\text{InAg}_{2/3}\text{V}_{1/3}\text{O}_3$ the ground state is non magnetic as shown in (f). In both cases, the bands just around the Fermi level are d_{z^2} from Cu for (e) and Ag for (f).

B. Non magnetic Ag based compound

A simple way to remove magnetism in this system is to substitute directly Cu by isoelectronic Ag. Doing this, we change from a 3d to a 4d electron system, with the corresponding increase in spin-orbit coupling strength and band width. The solution obtained for the compound $\text{InAg}_{2/3}\text{V}_{1/3}\text{O}_3$ is non-magnetic and its band structure is shown in Fig. 1f. The electron count is basically retained: $\text{V}^{5+}:d^0$, empty-shell nonmagnetic cations and $\text{Ag}^{2+}:d^9$ atoms with a single hole in the aforementioned d_{z^2} orbital, that becomes decoupled by the peculiar AgO_5 environment this structure presents. In this situation, the crystal-field energy that separates the d_{z^2} bands from the rest is even higher due to the more delocalized nature of the Ag 4d electrons, and hence this system becomes even more one-orbital-like. We can see that there is a 1.5 eV energy window around the Fermi level completely domi-

nated by the four Ag d_{z^2} bands in the unit cell. However the two Ag-rich planes show a sizable interaction due to their proximity, so that the low-energy properties are not the ones of two decoupled honeycomb lattices.

C. Dirac-like Ag-Zn based compound

In order to produce a single Dirac point in the band structure and change the topological properties of the system, one can try to remove this interaction between the active Ag layers by adding a spacing layer between them. Ideally, the preferred experimental situation would be to grow a single layer of this honeycomb lattice on the appropriate substrate (typically Al_2O_3 or some other hexagonal-based substrate like a wurtzite nitride AlN, e.g.). Another approach is to introduce a spacing layer based on full-shell $\text{Zn}^{2+}:\text{d}^{10}$ cations in the place of Ag (Figs. 2a,b). That way, interactions between the active Ag orbitals along the z -axis will be largely reduced and the problem becomes purely two-dimensional. Calculation of the orbital resolved density of states in Ag (Fig. 2c) confirms that in such situation the low-energy levels are still Ag d_{z^2} , showing also a strong mixing between the other d-orbitals away from the Fermi level (Fig. 2d).

In the situation described above, we can observe in Fig. 2a the band structure of that layered alternation of Zn-rich and Ag-rich planes in the two honeycombs that form the unit cell. Due to the lack of interaction between active Ag-rich planes, the low-energy spectrum are two Dirac cones close to the K and K' points, as expected from a simple one-orbital picture on a purely two-dimensional honeycomb lattice. Such electronic structure (see Fig. 2b) can be easily captured by means of Wannier procedure projecting onto the Ag d-orbitals, which gives rise to a tight binding Hamiltonian of the form

$$H_W = \sum_{i,j} t_{ij} c_j^\dagger c_i \quad (1)$$

where c_i and c_j^\dagger are (spinless) annihilation and creation operators in the d-like Wannier Ag orbitals, and $t_{i,j}$ are the hopping parameters obtained with the Wannierization procedure.

It is worth to mention that the underlying Ag honeycomb lattice has a small distortion due to a small dimerization between pairs of Ag sites. The effect of such structural feature is that the Dirac points are not strictly located in the K and K' points, but have a very small displacement in reciprocal space.^{31,32}

III. TOPOLOGICAL INSULATING STATE IN AG-ZN MULTILAYER

The calculations presented so far do not consider relativistic effects, so that the low-energy Hamiltonian of the

Ag-Zn compound are two gapless Dirac equations. In comparison, when SOC is included in the ab initio calculations, we observe that a gap opens up in the Dirac points (Fig. 3a). The former situation is analogous to the behavior of other Dirac materials as graphene, where an opening of the Dirac points by a perturbation which does not break time reversal symmetry nor inversion leads to a topological insulator of the Z_2 topological class.¹⁵

A. Topological invariant

In crystals with inversion symmetry, the non-triviality of the band structure can be easily checked by calculating the parities of the Khon-Sham eigenvalues.³³ However, the unit cell of the Ag-Zn compound no longer preserves inversion symmetry, invalidating the previous approach. To check that the band structure of this system is topologically non-trivial, we will instead take advantage of the tight binding Hamiltonian obtained previously. We generate a relativistic Hamiltonian by taking the Wannier Hamiltonian and adding SOC as an atomic term of the form $H_{SOC} = \lambda_{SOC} \vec{L} \cdot \vec{S}$. This leads to the following relativistic tight binding Hamiltonian

$$H_0 = H_W + H_{SOC} = \sum_{i,j,s} t_{ij} c_{j,s}^\dagger c_{i,s} + \sum_{i,j,s,s'} \lambda_{SOC} \vec{L}_{i,j} \cdot \vec{S}_{s,s'} c_{j,s}^\dagger c_{i,s'} \quad (2)$$

where t_{ij} are the (spinless) hopping parameters obtained from the Wannierization technique, $c_{i,s}$ and $c_{j,s'}^\dagger$ spinful annihilation and creation operators, \vec{L} the orbital angular momentum in the d-orbitals and \vec{S} the spin Pauli matrices. This approach allows to artificially control the strength of the SOC without having to perform further ab initio calculations. This is specially useful to understand the mechanism of gap opening as we will see later.

Upon introduction of SOC in the Wannier Hamiltonian we obtain a band structure showing a band gap (Fig. 3b), in agreement with the fully relativistic ab initio calculations (Fig. 3a). With the tight binding model, the non-triviality of the band gap can be probed by calculating the Z_2 invariant by means of the flow of Wannier charge centers.³⁴ Figure 3c confirms that the system is non-trivial because an odd number of crossings occurs along the variation of the chosen cyclic parameter, in this case the crystal momentum.

An interesting property of the gap of this system is that it depends linearly with the SOC strength (Fig. 3d), meaning that the channel that opens up the band gap enters as first order in SOC.³⁵ This is an important finding. Usually these oxides present a very small band gap since it opens up via second or third-order perturbations. That is the situation in perovskite (111) bilayers,²⁶ but here we see that the mechanism of gap opening in principle could allow for larger gaps to appear. It is crucial to understand what structures are prone to yield larger gaps,

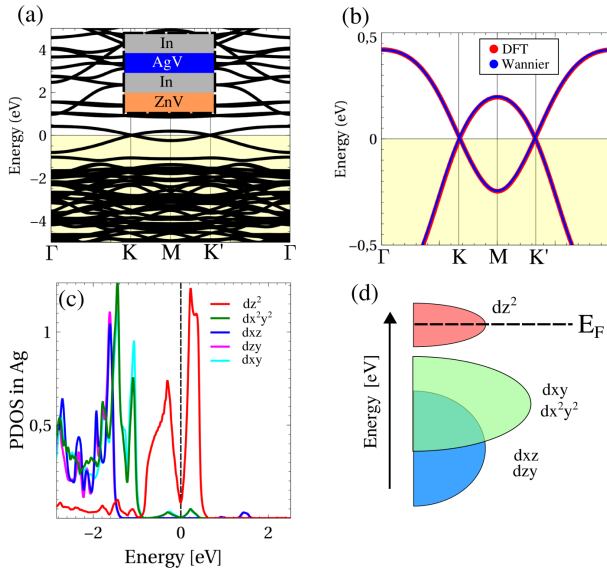


FIG. 2. (Color online.) (a) Non relativistic band structure of InZn_{1/3}Ag_{1/3}V_{1/3}O₃ calculated at the GGA level, where the low-energy properties are dominated by the single Ag layer. We observe that the Dirac point occurs close to the K point. Panel (b) shows a comparison of the low-energy bands between DFT and the tight binding model obtained through Wannierization. Although the electronic spectrum is Dirac-like, there is a strong electron-hole asymmetry. Projected density of states (c) over the Ag atom shows the dominant d_{z2} character of the Dirac bands, that can be understood with the simplified picture (d) considering the three oxygens in-plane create a local 120° rotation symmetry.

since these are required for applications, but so far these have been quite elusive, at least using oxides (with the exception of BaBiO₃,³⁶ which is however a metal if undoped). Being the band gap produced by SOC strength mainly, our DFT calculations show that it is quite insensitive to the exchange-correlation functional used, LDA or GGA yielding a very similar value close to 18 meV. Comparing with our tight-binding model, we can then extract the SOC strength by comparing the gap obtained with DFT and that from the model (see Fig. 3d), leading to a λ_{SOC} of about 150-170 meV, which is a large value but consistent with the atomic number of Ag.

B. Surface states

The direct consequence of the non-triviality of the band structure can be observed in finite geometries, where spin-polarized edge states show up. This can be easily checked with a tight binding model (in our case obtained from the Wannierization described above) by building up a finite system and calculating its electronic spectra. In particular, in a semi-infinite geometry two branches of edge states appear, which can be calculated

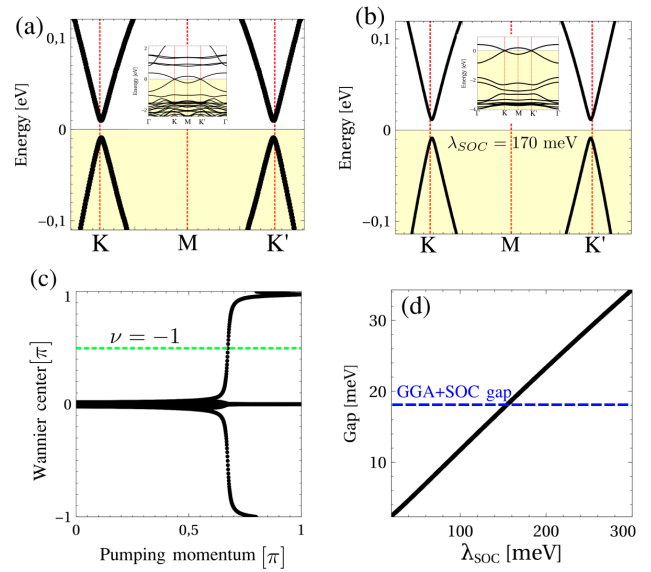


FIG. 3. (Color online.) Ab initio band structure (a) with spin-orbit coupling introduced in a fully relativistic manner by using the ELK code, showing a band gap opening close to the Dirac points. Panel (b) shows the band structure calculated using the tight-binding model obtained through Wannierization plus atomic SOC, which agrees very well with the one obtained from DFT. With the tight binding model, the flow of the Wannier charge centers, black dots in (c), is calculated as a function of a the other crystal momentum, which is used as pumping parameter. The fact that the Wannier centers cross the dashed green line an odd number of times proves the topological non-trivial nature of the band gap. Panel (d) shows the evolution of the gap with the SOC strength, showing a linear dependence and allowing for a determination of λ_{SOC} by comparing with the ab initio calculation.

by solving the Dyson equation for each Bloch Hamiltonian with wavevector parallel to the surface

$$G(k_x, E) = (E - h_0(k_x) - t(k_x)^\dagger G(k_x, E) t(k_x))^{-1} \quad (3)$$

where $h_0(k_x)$ is the k-dependent intracell hopping matrix and $t(k_x)$ the k-dependent intercell hopping matrix. From the surface Green function (Eq.3) the spectral density can be obtained as

$$\rho(k_x, E) = -\frac{1}{\pi} \text{Tr}[\text{Im}[G(k_x, E + i0^+)] \quad (4)$$

The previous k-dependent spectral function (see Fig. 4a) shows the two surface branches edge states expected for the semi-infinite geometry of a topological insulator. This shows the gapless edge states that appear well separated from the gapped bulk bands. Further insight on the topological properties of those states can be achieved by examining its spin polarization, which can be calculated from the spin spectral function

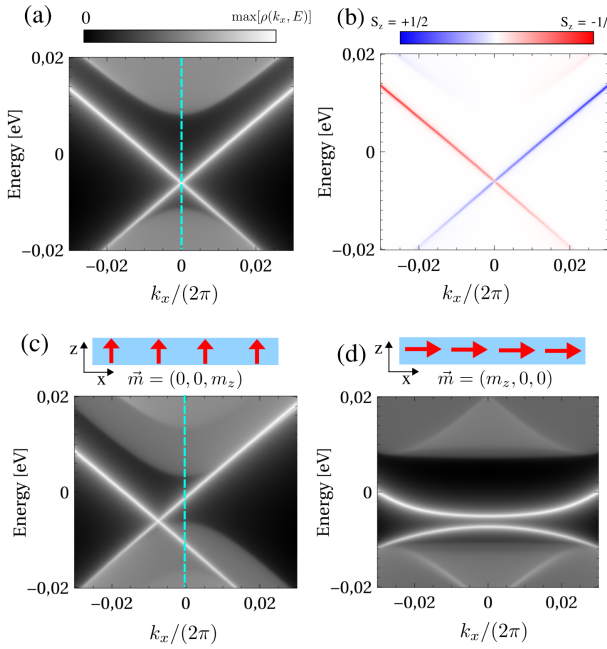


FIG. 4. (Color online.) Surface spectral function (a) in armchair like edge, showing two branches of gapless edge states plus the gapped bulk band structure. By calculating the spin character of those surface states (panel (b)), it is observed that they show opposite spin polarization as expected from a quantum spin Hall insulator due to spin-momentum locking. When time reversal is broken by a uniform exchange coupling, the conductance depends on the magnetization direction. For off-plane exchange $m_z = 2$ meV the edge states remain gapless (c), whereas for in-plane $m_x = 10$ meV they acquire a small gap (d).

$$\rho_z(k_x, E) = -\frac{1}{\pi} \text{Tr}[\text{Im}[S_z G(k_x, E + i0^+)] \quad (5)$$

where S_z is the spin Pauli matrix. This spin spectral function is shown in Fig. 4b, and it confirms the opposite spin polarization of the surface states that is produced by spin-momentum locking, typically obtained in QSHE systems like this.

The spin polarized states can be gapped out by perturbations that break time reversal symmetry, such as local exchange fields. That kind of perturbations can arise by interaction with a magnetic substrate, substitutional magnetic impurities or an external magnetic field. To understand the electronic properties in this situation, we study what is the effect on the surface edge states in the case that time reversal symmetry is broken. Under those circumstances, the bulk Z_2 invariant cannot be defined anymore, but we can gain some insight by studying the surface states of the semi-infinite system when adding a uniform local exchange to the Hamiltonian of the form:

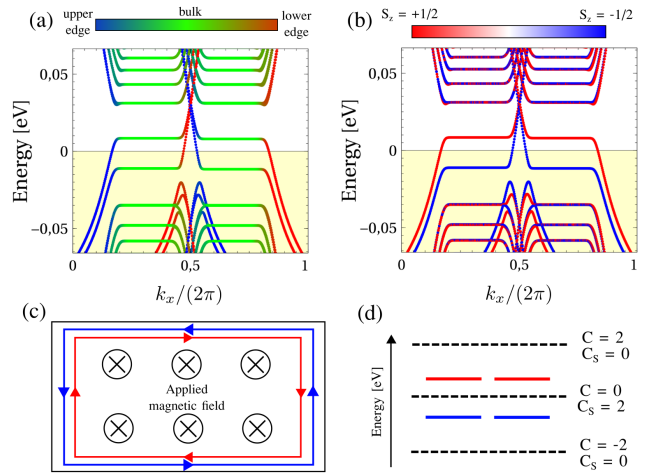


FIG. 5. (Color online.) (a) Band structure of a quantum Hall slab of the Ag-Zn compound, showing the position (a) and spin flavor (b) of the different eigenstates. The quantum spin Hall states survive even when time reversal symmetry is broken by a gauge magnetic field, and turns the system a ferromagnet even without interactions. Panel (c) shows a sketch of the quantum spin Hall configuration and (d) shows the different insulating states as function of the zero Landau level filling, quantum spin Hall at filling 0, and quantum Hall for filling ± 2 .

$$H = H_0 + H_Z = H_0 + \sum_{i,s,s'} \vec{m} \cdot \vec{S}_{s',s} c_{i,s'}^\dagger c_{i,s} \quad (6)$$

where H_0 is the Wannier Hamiltonian used previously.

We will consider two cases: when the magnetization is perpendicular to the Ag hexagonal plane, and when it is parallel. For perpendicular exchange, the nearly perfect spin polarization of the edge states allows them to be resilient to a gap opening, still showing gapless edge states (Fig. 4c). When the off-plane exchange field is large enough, the bulk gap closes leading to a topological metal, which has gapless edge states that coexist with normal conduction electrons. For in-plane exchange fields a gap opens up in the edge channels^{37,38} as shown in Fig. 4d, although the value of the gap opening is way smaller than the perturbation in this armchair edge. The bulk band structure remains gapped even when the in-plane exchange field becomes larger than the SOC gap. Something similar has been reported in oxides before: VO_2/TiO_2 multilayers^{22,39} have been shown to be Chern insulators⁴⁰ when magnetization is along the off-plane direction and open a trivial gap when the magnetization lies inside the plane.⁴¹

C. Quantum Hall effect

The Dirac-like low-energy spectra suggests that the system will show an unconventional Landau level (LL) spectrum very much like graphene. In the absence of SOC, the Dirac dispersion will yield a set of 4 zero Landau levels: one per spin and valley. The topological gap is equivalent to a mass in the K and K' points of the Brillouin zone that follows $m = s_z \kappa$, where s_z labels spin and κ labels valley. When a magnetic field is turned on, the zero Landau level will develop a splitting following $\Delta = m\kappa = s_z$, therefore independent on the valley. The previous splitting is equivalent to the one obtained in a Dirac ferromagnet^{42,43} but with the zero LL spin splitting coming from SOC instead of Zeeman, and automatically realizes the quantum spin Hall effect. Using the tight binding model derived before, we build a quantum Hall bar, where the magnetic field is included by means of the Peierls substitution $t_{ij} \rightarrow t_{ij}e^{i\phi_{ij}}$, with $\phi_{ij} = \frac{eB}{\hbar}(x_i - x_j)(y_i + y_j)$ and x_i, y_j the positions of the Wannier charge centers. The Zeeman term of the magnetic field is neglected provided that the splittings created by SOC are larger. The band structure obtained is shown in Fig. 5a,b, where the position and spin are represented by the color of the eigenvalue.

When the system is with the d_{z^2} manifold half filled, the spin-down zero LL are filled, whereas the spin-up are empty. In this situation, the Hall bar is the quantum spin Hall state, characterized by a spin Chern number $C_S = C_\uparrow - C_\downarrow = 2$, and two counter-propagating edge channels (Fig 5c). It is interesting to note that this quantum spin Hall state is not protected by time reversal symmetry but by conservation of S_z , and that the total Chern number is $C = 0$, so that the system will be vulnerable to perturbations creating spin mixing. In addition, this QSH state is adiabatically connected to the one occurring in the absence of SOC. When the Fermi energy is moved away from half filling (Fig. 5d) of the d_{z^2} states and all the zero Landau levels are filled, the system no longer realizes the QSH state. Instead, it enters into a normal quantum Hall state with $C = 2$ and two co-propagating edge states.

IV. CONCLUDING REMARKS.

To summarize, in this paper we present ab initio calculations on the oxide $\text{InZn}_{1/3}\text{Ag}_{1/3}\text{V}_{1/3}\text{O}_3$ based on the structure of the recently synthesized $\text{InCu}_{2/3}\text{V}_{1/3}\text{O}_3$. We have emphasized the Dirac-like low-energy electronic structure that occurs when magnetism is switched off and two-dimensionality is enforced. The low-energy properties, on both sides of the Fermi level, are shown to be dominated by Ag d_{z^2} orbitals. The unexpectedly simple low-energy effective model compares with the rather complex crystal structure and deep energy electronic mixing. In the same fashion of other Dirac materials, the inclusion of spin-orbit coupling leads to a topological insu-

lating state, with a band gap scaling linear with SOC strength. The non-triviality of the gap was confirmed by the calculation of the Z_2 invariant and edge states spectral functions. The study of this system provides some clues on how one can design topologicality using oxides, and in particular to understand how the topological gap can be tuned or even enhanced. We have compared the results obtained for this system with other oxide structures built from a honeycomb lattice, which can be even qualitatively very different. We have also analyzed the material using a tight-binding model obtained through a Wannierization procedure that fits perfectly the DFT bands around the Fermi level. Our calculations using the tight-binding Hamiltonian describe the behavior of such system in a quantum Hall experiment, and show that its properties would be very similar to the response of graphene, another single-band system (of p_z symmetry in that case) with honeycomb structure. Thus, this system we propose would be a close d-electron analogue of graphene.

ACKNOWLEDGMENTS

This work was supported by Xunta de Galicia under the Emerxentes Program via the project no. EM2013/037 and the MINECO via project MAT2013-44673-R. V.P. acknowledges support from the MINECO of Spain via the Ramon y Cajal program RyC-2011-09024. J. L. Lado acknowledges financial support by Marie-Curie-ITN Grant No. 607904-SPINOGRAPH.

V. COMPUTATIONAL PROCEDURES

Ab initio electronic structure calculations based on the density functional theory (DFT)^{44,45} have been performed using two all-electron full potential codes (WIEN2K⁴⁶ and ELK⁴⁷) and the pseudopotential-based Quantum Espresso code.⁴⁸ Unless stated otherwise, structural optimizations and band structure calculations were performed with GGA-PBE⁴⁹.

WIEN2K calculations were performed with a converged k -mesh, a value of $R_{mt}\text{K}_{max} = 7.0$, and spin-orbit coupling was introduced in a second variational manner using the scalar relativistic approximation.⁵⁰ Elk calculations were carried out with the non-collinear formalism and spin orbit coupling in order to calculate the topological gap as well as to check that the Ag based compound is non magnetic. Quantum Espresso calculations were carried out using PAW pseudopotentials.⁵¹ The structures were relaxed and the different approaches gave analogous results.

The Wannierization⁵²⁻⁵⁵ is performed in the non relativistic Quantum Espresso PAW calculation. The frozen window is chosen in the interval [-0.9,0.6] eV so that it contains the low energy d_{z^2} bands, whereas the outer window is chosen in the interval [-7,0.6] eV around the

Fermi energy. The projections used are the d-manifold of the Ag atoms, giving rise to a 10×10 tight binding Hamiltonian. Spin orbit coupling is included afterwards

as an $\vec{L} \cdot \vec{S}$ term in the Wannier tight binding model obtained, turning the Hamiltonian into a 20×20 matrix.

* jose.luis.lado@gmail.com

† victor.pardo@usc.es

- ¹ M. Z. Hasan and C. L. Kane, *Reviews of Modern Physics* **82**, 3045 (2010).
- ² X.-L. Qi and S.-C. Zhang, *Reviews of Modern Physics* **83**, 1057 (2011).
- ³ Y. Hatsugai, *Phys. Rev. Lett.* **71**, 3697 (1993).
- ⁴ D. Thouless, M. Kohmoto, M. Nightingale, and M. Den Nijs, *Physical Review Letters* **49**, 405 (1982).
- ⁵ L. Fu, *Physical Review Letters* **106**, 106802 (2011).
- ⁶ C. L. Kane and E. J. Mele, *Phys. Rev. Lett.* **95**, 146802 (2005).
- ⁷ D. Pesin and L. Balents, *Nature Physics* **6**, 376 (2010).
- ⁸ M. Dzero, K. Sun, V. Galitski, and P. Coleman, *Phys. Rev. Lett.* **104**, 106408 (2010).
- ⁹ L. Fu and C. L. Kane, *Phys. Rev. Lett.* **100**, 096407 (2008).
- ¹⁰ M. B. Hastings, C. Nayak, and Z. Wang, *Physical Review B* **87**, 165421 (2013).
- ¹¹ H. Jiang, S. Cheng, Q.-f. Sun, and X. C. Xie, *Phys. Rev. Lett.* **103**, 036803 (2009).
- ¹² D. Pesin and A. H. MacDonald, *Nature materials* **11**, 409 (2012).
- ¹³ C. Laflamme, M. Baranov, P. Zoller, and C. Kraus, *Physical Review A* **89**, 022319 (2014).
- ¹⁴ C. L. Kane and E. J. Mele, *Phys. Rev. Lett.* **95**, 146802 (2005).
- ¹⁵ C. L. Kane and E. J. Mele, *Phys. Rev. Lett.* **95**, 226801 (2005).
- ¹⁶ B. A. Bernevig and S.-C. Zhang, *Phys. Rev. Lett.* **96**, 106802 (2006).
- ¹⁷ M. König, S. Wiedmann, C. Brüne, A. Roth, H. Buhmann, L. W. Molenkamp, X.-L. Qi, and S.-C. Zhang, *Science* **318**, 766 (2007).
- ¹⁸ A. Shitade, H. Katsura, J. Kuneš, X.-L. Qi, S.-C. Zhang, and N. Nagaosa, *Phys. Rev. Lett.* **102**, 256403 (2009).
- ¹⁹ M. Kargarian, J. Wen, and G. A. Fiete, *Phys. Rev. B* **83**, 165112 (2011).
- ²⁰ J. Wang, R. Li, S.-C. Zhang, and X.-L. Qi, *Phys. Rev. Lett.* **106**, 126403 (2011).
- ²¹ J. F. Afonso and V. Pardo, *Phys. Rev. B* **92**, 235102 (2015).
- ²² V. Pardo and W. E. Pickett, *Phys. Rev. Lett.* **102**, 166803 (2009).
- ²³ T. Cai, X. Li, F. Wang, S. Ju, J. Feng, and C.-D. Gong, *Nano Letters* **15**, 6434 (2015).
- ²⁴ D. Xiao, W. Zhu, Y. Ran, N. Nagaosa, and S. Okamoto, *Nature Communications* **2**, 596 (2011).
- ²⁵ D. Doennig, W. E. Pickett, and R. Pentcheva, *Phys. Rev. B* **89**, 121110 (2014).
- ²⁶ J. Lado, V. Pardo, and D. Baldomir, *Physical Review B* **88**, 155119 (2013).
- ²⁷ A. Möller, U. Löw, T. Taetz, M. Kriener, G. André, F. Damay, O. Heyer, M. Braden, and J. A. Mydosh, *Phys. Rev. B* **78**, 024420 (2008).
- ²⁸ Y. Yan, Z. Li, T. Zhang, X. Luo, G. Ye, Z. Xiang, P. Cheng, L.-J. Zou, and X. Chen, *Physical Review B* **85**, 085102 (2012).
- ²⁹ M. Yehia, E. Vavilova, A. Möller, T. Taetz, U. Löw, R. Klingeler, V. Kataev, and B. Büchner, *Physical Review B* **81**, 060414 (2010).
- ³⁰ M. Bratsch, J. Tapp, A. P. Litvinchuk, and A. Moller, *Inorganic chemistry* **53**, 4994 (2014).
- ³¹ V. M. Pereira, A. C. Neto, and N. Peres, *Physical Review B* **80**, 045401 (2009).
- ³² M. Oliva-Leyva and G. G. Naumis, *Physical Review B* **93**, 035439 (2016).
- ³³ L. Fu and C. L. Kane, *Phys. Rev. B* **76**, 045302 (2007).
- ³⁴ A. A. Soluyanov and D. Vanderbilt, *Physical Review B* **83**, 235401 (2011).
- ³⁵ M. Gmitra, S. Konschuh, C. Ertler, C. Ambrosch-Draxl, and J. Fabian, *Physical Review B* **80**, 235431 (2009).
- ³⁶ B. Yan, M. Jansen, and C. Felser, *Nature Physics* **9**, 709 (2013).
- ³⁷ S. Rachel and M. Ezawa, *Physical Review B* **89**, 195303 (2014).
- ³⁸ J. L. Lado and J. Fernández-Rossier, *Phys. Rev. Lett.* **113**, 027203 (2014).
- ³⁹ S. Banerjee, R. R. P. Singh, V. Pardo, and W. E. Pickett, *Phys. Rev. Lett.* **103**, 016402 (2009).
- ⁴⁰ H. Huang, Z. Liu, H. Zhang, W. Duan, and D. Vanderbilt, *Phys. Rev. B* **92**, 161115 (2015).
- ⁴¹ V. Pardo and W. E. Pickett, *Phys. Rev. B* **81**, 035111 (2010).
- ⁴² A. F. Young, C. R. Dean, L. Wang, H. Ren, P. Cadden-Zimansky, K. Watanabe, T. Taniguchi, J. Hone, K. L. Shepard, and P. Kim, *Nature Physics* **8**, 550 (2012).
- ⁴³ H. A. Fertig and L. Brey, *Phys. Rev. Lett.* **97**, 116805 (2006).
- ⁴⁴ P. Hohenberg and W. Kohn, *Phys. Rev.* **136**, B864 (1964).
- ⁴⁵ W. Kohn and L. J. Sham, *Phys. Rev.* **140**, A1133 (1965).
- ⁴⁶ K. Schwarz and P. Blaha, *Comp. Mat. Sci.* **28**, 259 (2003).
- ⁴⁷ <http://elk.sourceforge.net/>.
- ⁴⁸ P. Giannozzi, S. Baroni, N. Bonini, M. Calandra, R. Car, C. Cavazzoni, D. Ceresoli, G. L. Chiarotti, M. Cococcioni, I. Dabo, *et al.*, *Journal of Physics: Condensed Matter* **21**, 395502 (2009).
- ⁴⁹ J. P. Perdew, K. Burke, and M. Ernzerhof, *Phys. Rev. Lett.* **77**, 3865 (1996), **78**, 1396(E) (1997).
- ⁵⁰ D. J. Singh, *Planewaves, pseudopotentials and LAPW method* (Kluwer Academic Publishers, 1994).
- ⁵¹ G. Kresse and D. Joubert, *Physical Review B* **59**, 1758 (1999).
- ⁵² A. A. Mostofi, J. R. Yates, Y.-S. Lee, I. Souza, D. Vanderbilt, and N. Marzari, *Computer physics communications* **178**, 685 (2008).
- ⁵³ N. Marzari and D. Vanderbilt, *Physical review B* **56**, 12847 (1997).
- ⁵⁴ I. Souza, N. Marzari, and D. Vanderbilt, *Physical Review B* **65**, 035109 (2001).
- ⁵⁵ N. Marzari, A. A. Mostofi, J. R. Yates, I. Souza, and D. Vanderbilt, *Reviews of Modern Physics* **84**, 1419 (2012).